ORIGINAL RESEARCH

Apoptotic Vesicles Attenuate Acute Lung Injury *via* CD73-Mediated Inhibition of Platelet Activation and NETosis

Lingping Tan [ID][1,2,]*, Chi Zhang[1,2,]*, Xiaoxing Kou[1−3], Lu Zhao[4], Di Wu[1−3], Jinyu Li[1,2], Chuanying Yu[1,2], Tansi Xu[1,2], Li Gao[1,2], Xueli Mao[1−3], Chuanjiang Zhao [ID][1,2]

[1]Hospital of Stomatology, Guanghua School of Stomatology, Sun Yat-sen University, Guangzhou, People's Republic of China; [2]Guangdong Provincial Key Laboratory of Stomatology, Guangzhou, People's Republic of China; [3]South China Center of Craniofacial Stem Cell Research, Guangzhou, People's Republic of China; [4]Department of Orthodontics, Affiliated Stomatology Hospital of Guangzhou Medical University, Guangdong Engineering Research Center of Oral Restoration and Reconstruction, Guangzhou Key Laboratory of Basic and Applied Research of Oral Regenerative Medicine, Guangzhou, Guangdong, People's Republic of China

*These authors contributed equally to this work

Correspondence: Chuanjiang Zhao, Department of Periodontology, Hospital of Stomatology, Sun Yat-sen University, Guangzhou, Guangdong, 510055, People's Republic of China, Email zhaochj@mail.sysu.edu.cn; Xueli Mao, South China Center of Craniofacial Stem Cell Research, Guanghua School and Hospital of Stomatology, Sun Yat-sen University, Guangzhou, Guangdong, 510080, People's Republic of China, Email maoxuel@mail.sysu.edu.cn

Introduction: Acute respiratory distress syndrome (ARDS) is a life-threatening type of acute lung injury (ALI) characterized by elevated mortality rates and long-term effects. To date, no pharmacological treatment has proven effective for ARDS. Mesenchymal stem cell-derived apoptotic vesicles (apoVs) were recently found to have excellent therapeutic potential for inflammatory diseases. In this study, our aim was to investigate the therapeutic effects and underlying mechanisms of apoVs in ALI.

Methods: ALI was induced in mice through intratracheal instillation of lipopolysaccharide (LPS). ApoVs were then administered two hours post-induction, and their impacts on platelet activation, neutrophil infiltration, and NETosis were assessed. Additionally, the role of CD73 in mediating these effects was thoroughly investigated.

Results: ApoVs inhibit platelet activation, thereby impeding the infiltration of neutrophils into the lung and the initiation of NETosis, ultimately alleviating ALI. Remarkably, apoVs were enriched with CD73, which was critical for apoV-mediated repression of platelet activation and neutrophil NETosis, as well as the therapeutic effects observed in lung injury.

Conclusion: This study reveals that apoVs inhibit platelet activity and neutrophil NETosis via CD73, offering an innovative and effective cell-free therapeutic strategy for ALI/ARDS.

Keywords: apoptotic vesicle, NETosis, platelet, ALI, CD73

Introduction

Acute respiratory distress syndrome (ARDS) is a severe form of acute lung injury (ALI) with high mortality rates.[1] Characterized by diffuse lung injury, leukocyte infiltration and gas exchange impairment.[2,3] ARDS may also cause long-term muscle weakness or cognitive impairment in patients who survive the acute phase of the disease.[4] Despite extensive research, there is still no effective pharmacotherapy for ARDS. Mesenchymal stem cell (MSC)-based therapy has been proposed as a potential treatment due to its anti-inflammatory and immunomodulatory properties.[5−9] However, the underlying mechanism of MSC-based therapy is still unclear. Recent evidence suggests that MSCs undergo apoptosis and release apoptotic vesicles (apoVs) into the host circulation or engrafted tissues, and this apoptotic process is necessary for the inflammatory regulation and immunosuppression functions of MSCs.[10,11] ApoVs, which contain DNA, RNA, proteins, and organelles,[12] have been reported to have significant potential as a cell-free therapy.[13,14] However, whether apoVs possess therapeutic potential for ALI/ARDS remains to be elucidated.

Graphical Abstract
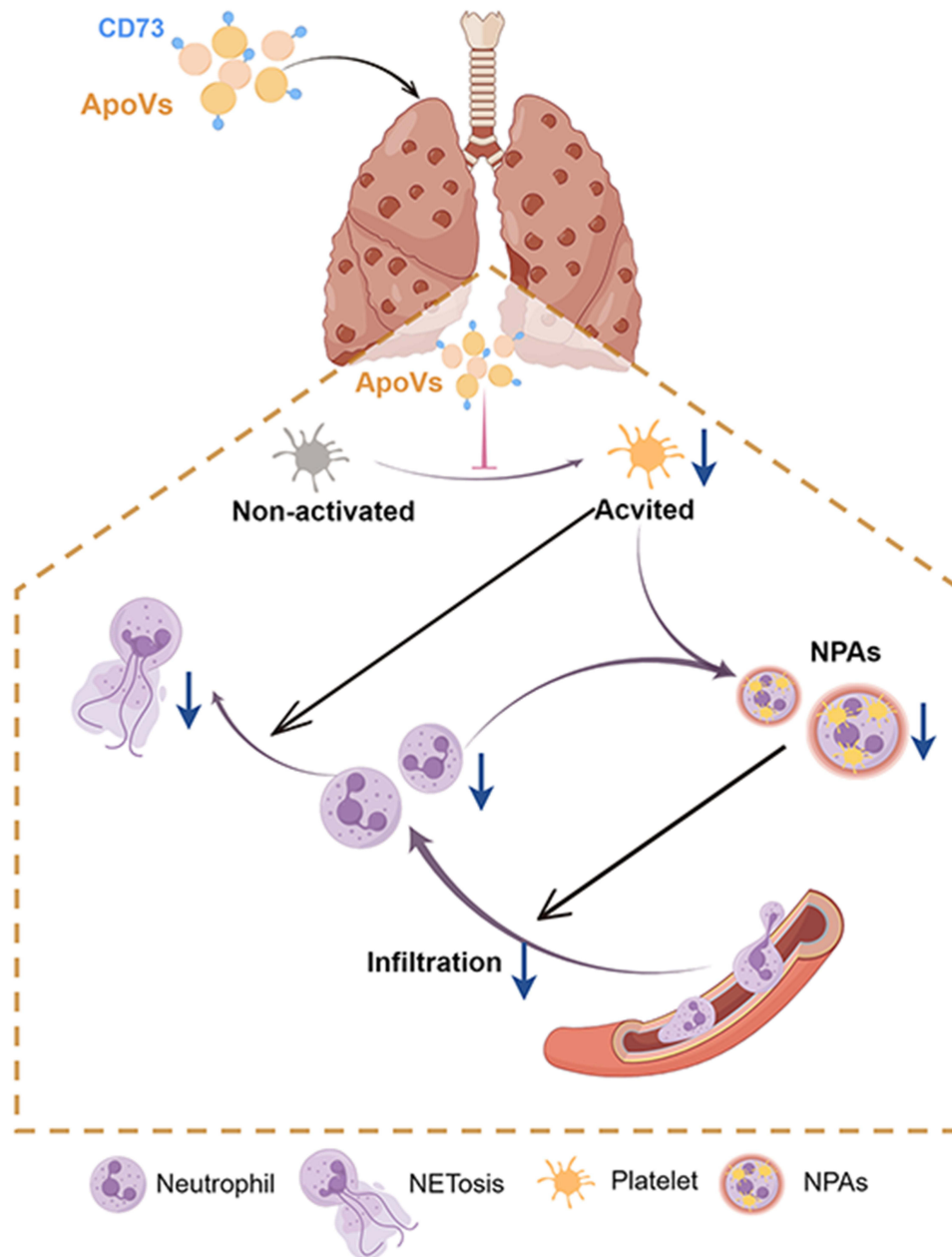
Studies on ALI/ARDS have consistently identified neutrophils as key cellular mediators of the early innate immune response.[15,16] In the context of ALI/ARDS, neutrophils have been shown to exhibit increased chemotaxis, activated metabolism, and delayed apoptosis.[17,18] As neutrophils migrate across the epithelium, they release toxic mediators and undergo NETosis, which involves the creation of neutrophil extracellular traps (NETs) to eliminate the insult.[19] However, NETosis can cause bystander damage, exacerbating tissue damage[20] and promoting a prothrombotic state that further activates platelets.[21] Therefore, we aimed to investigate whether apoVs can reduce the severity of ALI/ARDS by controlling the biological behavior of neutrophils.

Pulmonary endothelial injury in ARDS triggers platelet activation, which in turn promotes proinflammatory responses and induces thrombosis, thereby exacerbating endothelial injury.[22] Activated platelets also secrete chemokines and interact with neutrophils, resulting in neutrophil chemotaxis and NETosis in the injured lung, further aggravating lung injury.[23] It has been reported that some MSCs can inhibit platelet activation and aggregation through CD73.[24–26] CD73 is a homodimeric glycosylphosphatidylinositol (GPI)-anchored enzyme that converts AMP to adenosine. Adenosine activates adenosine receptors, triggering diverse signal transduction pathways that suppress platelet activation and inflammation.[27] To date, it remains unclear whether apoVs can attenuate neutrophil activation by inhibiting platelet activation through CD73.

This study demonstrated that intratracheal administration of MSC-derived apoVs could ameliorate inflammatory injury in mice with ALI. The beneficial effect of apoVs is probably attributable to the CD73-dependent inhibition of platelet activation and suppression of neutrophil NETosis. This finding reveals a potential cell-free therapeutic strategy for lung injury in ALI/ARDS patients.

Material and Methods

Animals

Eight-week-old male C57BL/6 mice were purchased from the Guangdong Medical Laboratory Animal Center and used for all animal experiments. Animals were grouped using a method of randomization. Animals used in this study were maintained in accordance with the Guideline for ethical review of animal welfare of laboratory animals published by the China National Standardization Management Committee (publication No. GB/T 35892–2018). Animal experiments were approved by the Institutional Animal Care and Use Committee of Sun Yat-sen University (SYSU-IACUC-2021-000434).

Cells

Human bone marrow MSCs (BMMSCs) (Cat. No. 7500) were purchased from ScienCell (San Diego, CA, USA). BMMSCs were cultured in α-MEM supplemented with 15% FBS, 100 U/mL penicillin, 100 mg/mL streptomycin, 2 mM L-glutamine, and 0.1 mM L-ascorbic acid phosphate at 37°C in a humidified tissue culture incubator with 5% CO_2. The culture medium was replaced every 3 days. When the cells reached 90% confluency, cells were digested with TrypLE Express Enzyme (Thermo Fisher Scientific, Waltham, America) for subsequent passaging. In the experiments, BMSCs were used at P3- P6. The characteristics of the BMMSCs were verified by colony-forming unit assays, cell morphology evaluations, osteogenic differentiation assays, adipogenic differentiation assays, and surface marker expression analysis.

For osteogenic differentiation, once the cells reached approximately 90% confluency, the culture medium was replaced with osteogenic induction medium containing 1.8 mM monopotassium phosphate, 10 nM dexamethasone, 100 U/mL penicillin, 100 mg/mL streptomycin, 0.1 mM L-ascorbic acid phosphate, 2 mM L-glutamine, 15% fetal bovine serum, and α-MEM culture medium. Osteogenic induction medium was refreshed every 3 days. After 14 days of differentiation, the cultured cells were stained with alizarin red.

For adipogenic differentiation, once the cells reached approximately 90% confluency, the culture medium was replaced with adipogenic induction medium for 3 days and followed by 1 day in maintenance medium. This cycle was repeated, and after 20 days, the cells were cultured in maintenance medium for an additional 4 days. Subsequently, the cells were stained with Oil Red O.

Antibodies and Reagents

Antibodies against TNF-α (#ab1793), IL-6 (#ab6672), citrullinated histone H3 (H3Cit #ab5103), Alix (#ab275377) and CD73 (#ab133582) were purchased from Abcam (Cambridge, MA, USA). Antibodies against Ly6G (#GB11229) and myeloperoxidase (MPO, #GB12224) were purchased from Servicebio (Wuhan, China). Antibodies against cleaved caspase 3 (c-caspase 3, #9664), caspase 3 (#9662), and calreticulin (#12238s) were purchased from Cell Signaling Technology (Waltham, MA, USA). Antibodies against CD9 (#sc-13118) and the CD73 inhibitor AMP-CP (#sc-214457) were purchased from Santa Cruz Biotechnology (Santa Cruz, CA, USA).

The Ly6G-PE (#127608), CD11b-APC/Cyanine7 (#101226), CD61-FITC (#104305), CD61-PE (#104307) and CD62P-APC (#148303) antibodies were purchased from BioLegend. The CD29-PE (#556049), CD73-PE (#550257), CD90-PE (#561970), CD105-PE (#560839), CD146-PE (#550315), CD166-PE (#559263), CD34-FITC (#555821), CD45-PE (#555483) antibodies and Annexin V-FITC (#556419) were purchased from BD Biosciences (San Jose, CA, USA). LPS (#3024) and the antibody against β-actin (#A5441) were purchased from Sigma-Aldrich (St. Louis, MO, USA). Staurosporine (STS, #ALX-380-014) was purchased from Enzo Life Sciences (Farmingdale, NY, USA). Phorbol 12-myristate 13-acetate (PMA, #1652981) was purchased from BioGems (Westlake Village, CA, USA). Adenosine diphosphate (ADP, #23811000) and collagen (#23802100) were purchased from SINNOWA Co. (Nanjing, China). Collagenase type I (#LS004197) was purchased from Worthington (Lakewood, NJ, USA). Dispase II (#04942078001) was purchased from Roche (Basel, Switzerland). Adipogenic differentiation and staining kit (#WWL-G040) was purchased from Shanghai Fuheng Biotechnology (Shanghai, China). The mouse bone marrow neutrophil isolation kit (#P8550) was purchased from Solarbio Science Technology (Beijing, China).

Isolation and Characterization of apoVs

ApoVs are produced during cellular apoptosis. To induce apoptosis, BMMSCs were treated with 500 nM STS for 6 hours. Then, apoVs were isolated by sequential centrifugation. Briefly, after centrifugation at 800 ×g for 10 min to remove cells and debris, the supernatant was centrifuged at 2000 ×g for 10 min. Then, the supernatant was further centrifuged at 16000 ×g for 30 min, and the pellet was washed twice in phosphate-buffered saline (PBS). The size distribution of apoVs was measured with a ZetaView PMX120 (Particle Metrix, Germany), and the morphological features of the apoVs were observed with a transmission electron microscope (TEM) (JEOL, Japan). The expression of annexin V in apoVs was examined by immunofluorescence staining with a confocal microscope (Carl Zeiss, Oberkochen, Germany) and flow cytometry with a NovoCyte flow cytometer (Agilent, Xian, China). The protein expression levels of caspase 3 and c-caspase 3 in apoVs were measured by Western blotting.

LPS-Induced ALI Mouse Model

An ALI mouse model was established by administering LPS via intratracheal instillation.[28] After the mice were anesthetized, LPS was injected into the trachea at a dose of 5 mg/kg to induce ALI. Two hours after LPS administration, apoVs (1×10^{10} particles in 20 μL of PBS for each mouse) were injected into the mice in the LPS+ apoV group via intratracheal instillation. The mice with ALI received 20 μL of PBS instead of apoVs. At 24 hours after LPS administration, the lungs of all the mice were scanned with a microCT scanner (PINGSENG Healthcare, China), and the mice were then sacrificed. Blood, lung, and bronchoalveolar lavage fluid (BALF) samples were harvested for subsequent experiments.

Tissue and BALF Collection

The lungs were collected for histological evaluation, analysis of the lung wet/dry weight ratio, and protein extraction. For BALF collection, a catheter (Carelife Co. Ltd., China) was inserted into the trachea, and then the lungs were flushed with 1 mL of PBS. Next, approximately 0.7 mL of BALF was retrieved.[29] The BALF was centrifuged at 500 × g for 5 min, and the supernatant was collected for protein concentration analysis.

Measurement of the Lung Wet/Dry Ratio

One lobe of the right lung harvested from the mice in each group was used for the wet/dry weight ratio calculation. Briefly, the lung tissues were harvested and weighed immediately, and the wet weight was recorded. Then, the lung tissues were placed in an oven at 60°C for 24 hours and weighed to determine the dry weight. The lung wet/dry ratio was calculated by dividing the wet weight by the dry weight.[30]

Histological Analysis

For lung injury analysis, the lung tissue was fixed in 4% paraformaldehyde, dehydrated, embedded in paraffin, cut into 5-μm-thick sections, and stained with hematoxylin and eosin (H&E). The evaluation was performed in a blinded manner.

Three random fields of view of each lung tissue sample at high power (40×) were chosen for scoring. The following variables were assessed: (A) neutrophils in the alveolar space (none = 0, 1–5 cells = 1, > 5 cells = 2), (B) neutrophils in the interstitial space/septa (none = 0, 1–5 cells = 1, > 5 cells = 2), (C) hyaline membranes (none = 0, one membrane = 1, > 1 membrane = 2), (D) proteinaceous debris in the air spaces (none = 0, one instance = 1, > 1 instance = 2), and (E) alveolar septal thickening (< 2× mock thickness = 0, 2–4× mock thickness = 1, > 4× mock thickness = 2). To obtain the lung injury score, the scores for A–E were then entered into the following formula, which contains multipliers that assign different levels of importance for each phenotype associated with the disease state: score = [(20 × A) + (14 × B) + (7 × C) + (7 × D) + (2 × E)]/100. Then, the scores for the three fields of view per mouse were averaged to obtain the final score.[31]

Immunofluorescence Staining

Lung tissue samples were fixed in 4% paraformaldehyde, dehydrated with 30% saccharose, embedded in optimal cutting temperature (OCT) compound (Leica, Germany) and cut into 8-μm-thick frozen sections. The cells were fixed in 4% paraformaldehyde. Then, the samples were permeabilized with 0.1% Triton X-100 in PBS. After being blocked with 5% bovine serum albumin (BSA), the samples were incubated with primary antibodies (antibodies specific for mouse TNF-α, IL-6, Ly6G, H3Cit, MPO, CD61 and annexin V) at 4°C overnight. Next, the sections were incubated with an Alexa Fluor-conjugated secondary antibody (Invitrogen, Carlsbad, CA, USA) at room temperature for 1 hour. After being washed, the cells were counterstained with 4',6-diamidino-2-phenylindole (DAPI). Images of the samples were acquired by confocal microscopy, and the images were evaluated with ImageJ software.

Immunohistochemical Staining

Paraffin-embedded lung tissue sections were deparaffinized and rehydrated. After antigen retrieval with citrate, endogenous peroxidase in the samples were blocked with 3% H_2O_2 for 30 min at room temperature. The samples were then blocked with 5% BSA for 30 min and incubated with a primary antibody specific for Ly6G at 4°C overnight. Then, the sections were incubated with the corresponding biotinylated secondary antibody (Santa Cruz Biotechnology) for 1 hour at room temperature and with the avidin-biotin-peroxidase complex (ABC Elite Kit, PK-6200, Vector Labs) for an additional 30 min. After the sections were incubated with diaminobenzidine solution (DAB, SK-4100, Vector Labs), they were counterstained with hematoxylin. All tissues were observed and images were recorded with a light microscope (Carl Zeiss, Oberkochen, Germany).

Enzyme-Linked Immunosorbent Assay (ELISA)

The serum of the mice was collected after the blood was centrifuged at 1000 × g for 15 min and stored at −80°C. The cytokine interleukin (IL)-10 in the serum was measured by ELISA (Maisha Industries Limited Company, Yancheng, China) according to the manufacturer's instructions.

Flow Cytometry

Lung tissue cells were collected via enzymatic digestion. Briefly, lung tissue was minced and digested with 3 mg/mL collagenase type I and 4 mg/mL dispase II for 1 hour at 37°C. Then, the dissociated cell suspension was filtered through a 70 mm cell strainer. Red blood cells were lysed using red blood cell lysis buffer. The harvested cells were washed with ice-cold PBS.

To investigate the infiltration of neutrophils into the lungs, lung tissue cells were collected, stained with Ly6G-PE and CD11b-APC/Cyanine7 antibodies for 20 min, and subjected to flow cytometry analysis.

To investigate neutrophil NETosis, the cells were fixed and permeabilized for 30 min, incubated with a primary antibody against H3Cit for 1 hour, incubated with an Alexa Fluor 488-conjugated secondary antibody for 30 min, incubated with a Ly6G-PE antibody for 20 min, and then subjected to flow cytometry analysis.

Assessment of Platelet Activation

Blood samples were collected in sodium citrate anticoagulant tubes and centrifuged at 300 × g for 10 min. The supernatant was collected and centrifuged at 3000 × g for 15 min. The platelets were in the precipitate. To evaluate

platelet activation in vivo, platelets from mice in different groups were collected, stained with CD61-PE and CD62P-APC antibodies at 37°C for 30 min and then evaluated by flow cytometry analysis.

To evaluate platelet activation in vitro, platelets were collected and adjusted to 300000platelets/µL with platelet-poor plasma from the same mouse. In the activated groups, the platelets were treated with ADP or collagen for 5 min, while the platelets in the apoV-treated groups were treated with ADP/collagen and apoVs for 5 min. CD73 inhibitor-treated apoVs were pretreated with AMP-CP for 15 min. Then, the platelets were collected, stained with CD61-PE and CD62P-APC antibodies and subjected to flow cytometry analysis.

Platelet aggregations were tested using a PL-12 platelet function analyzer (SINNOWA Co., Nanjing, China). Platelet aggregations were tested by automatically and sequentially counting platelet numbers in the citrated whole blood sample before and after adding agonists at fixed time intervals. According to the instructions, blood sample was transferred to a polycarbonate tube for detection. The platelet count was detected and automatically set as the baseline. Then, agonists or agonists and apoVs were added to the blood samples from the experimental groups. Blood samples from one mouse were divided into three groups (control, agonists and agonists + apoVs) or five groups (control, agonists, agonists + apoVs, agonists+ $CD73^{KD}$-apoVs and agonists + inhibitor + apoVs). After the test, a PL-12 platelet function analyzer reported a series of parameters for the samples, including the maximum aggregation ratio (MAR%) and average aggregation ratio (AAR%) of platelets.[32,33]

Isolation of Neutrophils

Neutrophils were isolated from the bone marrow of C57BL/6 mice using a mouse bone marrow neutrophil isolation kit. In brief, bone marrow was flushed out from the tibias and femurs using RPMI 1640 medium supplemented with 10% FBS, followed by preparation of a single-cell suspension at a density of 2×10^8-1×10^9 cells/mL. Neutrophils were subsequently purified from the single-cell suspension following to the manufacturer's instructions. The isolated neutrophils were cultured in RPMI 1640 medium supplemented with 10% FBS, 100 U/mL penicillin, 100 mg/mL streptomycin and 2 mm L-glutamine.

For NETosis induction experiments, neutrophils were stimulated with platelets for 4 hours.

Assessment of Neutrophil NETosis

A co-culture system of platelets and neutrophils was established to investigate the effect of activated platelets on NETosis. Platelets were pretreated based on designated experimental groups and subsequently co-cultured with neutrophils for 4 hours. Following co-culture, the level of NETosis was evaluated. The methods for platelet pretreatment were consistent with those described in the "Assessment of Platelet Activation" section. The experimental groups were as follows: control, ADP-treated platelets, ADP+apoV-treated platelets, ADP+$CD73^{KD}$ -apoV-treated platelets, and ADP +inhibitor+apoV-treated platelets.

Identification of Key Effector Proteins on apoVs

We utilized the "clusterProfiler" package in R software to convert UniProt IDs originating from proteomic analysis of apoVs from BMMSCs into NCBI Gene Symbols. Then, we downloaded the 'GOBP_ADENOSINE_METABOLIC_PROCESS' gene set from the Molecular Signatures Database (MSigDB). Venn diagrams were subsequently generated to identify the consensus adenosine metabolic enzymes within the apoV.

Transfection of Small Interfering RNA into BMMSCs

For CD73 knockdown, BMMSCs were transfected with siRNA-CD73 (siCD73, RiboBio, Guangzhou, China) or siRNA-negative control (siControl) using Lipofectamine RNAiMAX transfection reagent (Thermo Fisher Scientific, Waltham, MA, USA) following the manufacturer's instructions. Transfection efficiency was evaluated by RT–qPCR, flow cytometry and Western blotting.

Quantitative Real-Time Polymerase Chain Reaction

The transfection efficiency of siCD73 was determined by RT–qPCR. Briefly, MSCs were harvested, and total RNA was extracted using an RNA-Quick Purification Kit (ESscience, Shanghai, China). Subsequently, mRNA was reverse transcribed into cDNA by Primescript II RTase (Takara, Otsu, Japan). RT–qPCR was performed on a Light Cycler System (LightCycler, Roche Diagnostics) with a TB Green Premix Ex Taq II kit (Takara, Otsu, Japan). Gene expression was calculated via the $2^{-\Delta\Delta CT}$ method. The housekeeping gene GAPDH was used to normalize mRNA levels. The primers used in this study are shown in Table S1 in the Supplementary Material.

Western Blotting

Cells or apoVs were harvested and lysed in RIPA buffer on ice for 30 min. Total protein concentrations were measured with a Pierce BCA protein assay kit (Thermo Scientific, Waltham, MA, USA). Equal amounts of protein for each sample were separated via sodium dodecyl sulfate–polyacrylamide gel electrophoresis and transferred to polyvinylidene fluoride membranes. Subsequently, the membranes were blocked with 5% BSA for 1 hour at room temperature and incubated overnight at 4°C with primary antibodies specific for Ly6G, MPO, H3Cit, caspase 3, c-caspase 3 and β-actin. The membranes were incubated with horseradish peroxidase-conjugated secondary antibodies for 1 hour. The protein bands were detected with an imaging system (Bio-Rad Laboratories, Hercules, CA, USA). The protein expression levels were normalized to those of β-actin.

Statistical Analysis

GraphPad Prism 8 (GraphPad Software, USA) was used to perform statistical and generate graphs. According to the homogeneity test of variance, comparisons among more than two groups were analyzed using one-way analysis of variance (ANOVA) with Tukey's post hoc test. All data are expressed as the mean ± standard deviation (SD). $P < 0.05$ was considered to indicate statistical significance.

Results

Intratracheal Administration of MSC-Derived apoVs Attenuated Acute Lung Injury in Mice with ALI

The human BMMSCs used in our study were identified by their colony formation ability, typical fibroblast-like morphology, osteogenic and adipogenic differentiation capability, and expression of MSC surface markers (Figure S1A-E). ApoVs were isolated from MSCs using a sequential centrifugation process, as previously reported[13,14] and exhibited a double-membrane spherical structure when observed via transmission electron microscopy (TEM) (Figure S1F). Nanoparticle tracking analysis revealed that the size of apoVs ranged from 50−250 nm (average size of 165 nm) (Figure S1G). Immunofluorescence staining and flow cytometry analysis revealed that the apoVs were positive for the apoV-specific marker phosphatidylserine (indicated by Annexin V staining) (Figure S1H and I). To further confirm the purity of apoVs, Western blotting was performed, which revealed that apoVs expressed specific apoptosis-associated markers, such as c-caspase 3 and calreticulin, as well as common EV markers, such as CD9 and Alix (Figure S1J). These results were consistent with previous studies and verified the characteristics of apoVs.[14]

To investigate the effects of apoVs on lung injury, mice with LPS-induced ALI were treated with MSC-derived apoVs at 2 hours post-LPS injury (Figure 1A). Histological analysis revealed that the mice with ALI exhibited typical features of ALI, such as diffuse alveolar damage, numerous infiltrating neutrophils, alveolar congestion, hemorrhage, and interstitial edema (Figure 1B). We discovered that both systemic infusion and intratracheal administration of apoVs significantly ameliorated lung injury, as evaluated by H&E staining and lung injury scoring (Figure 1B, and C and Figure S2A and B). In addition, mice with ALI exhibited impaired lung alveolar-capillary membrane conductance, as indicated by increased lung wet/dry ratios and total protein concentrations in the BALF (Figure 1D and E). However, systemic infusion and intratracheal administration of apoVs rescued mice with ALI from lung alveolar-capillary membrane injury (Figure 1D and E and Figure S2C and D). Subsequently, we used PKH26-labeled apoVs to show that a greater lung distribution of apoVs was detected in the mice subjected to intratracheal administration than in the mice subjected to
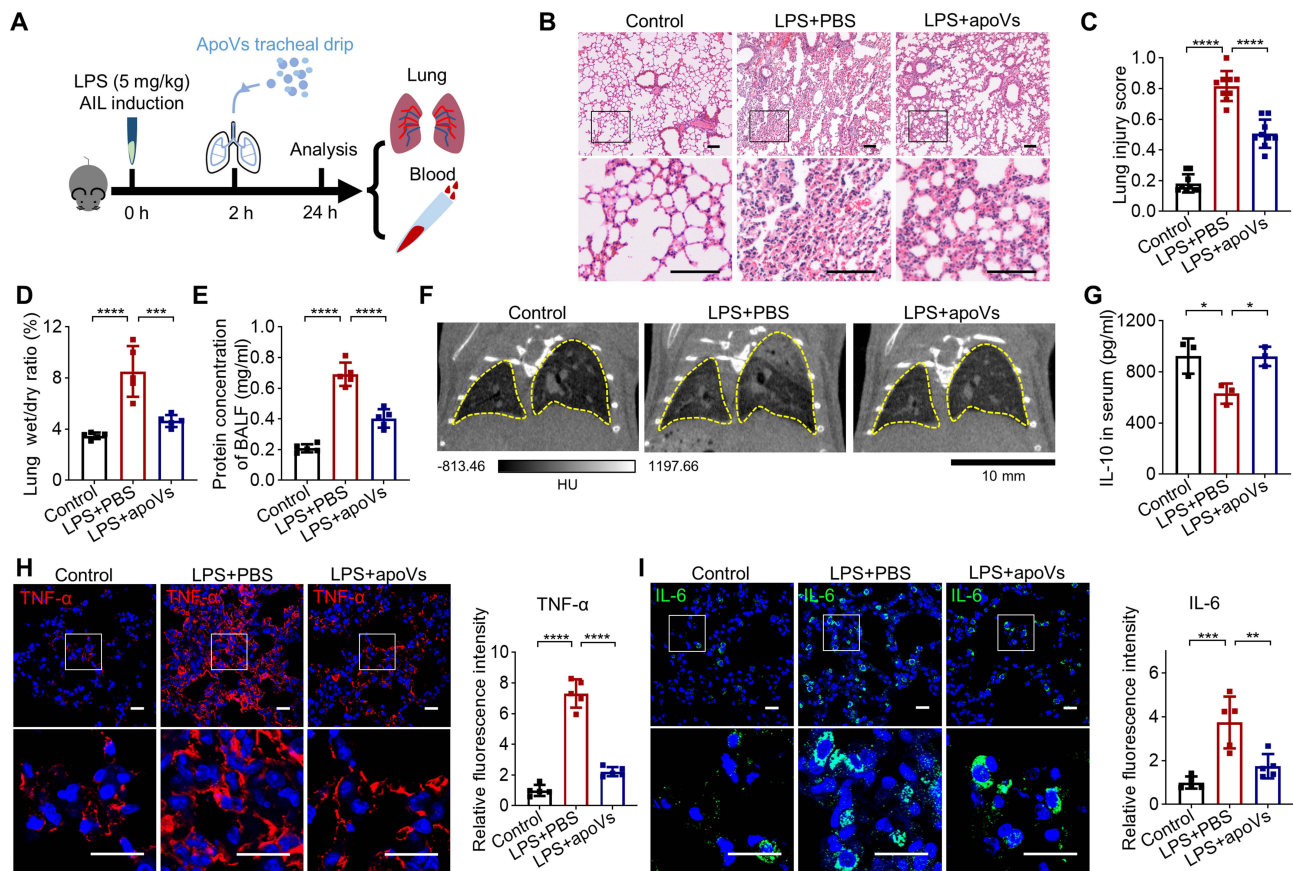
Figure 1 Intratracheal administration of BMMSC-derived apoVs attenuated lung injury in the ALI mouse model. (**A**) The schematic diagram shows the approach used for treatment of the ALI mouse model with BMMSC-derived apoVs. (**B**) Representative H&E staining of lung samples. Compared with ALI induction, apoV treatment significantly alleviated lung injury in mice. Bar = 100 μm. (**C**) The lung injury scores were lower in the mice that received apoV treatment than in the mice with ALI (*n*=9). (**D**) The lung wet/dry ratios showed that apoV treatment attenuated LPS-induced lung edema (*n*=5). (**E**) Protein concentrations in BALF from different groups (*n*=5). (**F**) Representative micro-CT images of the lung showing that apoV treatment rescued the ALI. (**G**) Serum IL-10 levels increased after apoV treatment (*n*=3). (**H, I**) Immunofluorescence staining of lung samples revealed significantly increased concentrations of TNF-α (**H**) and IL-6 (**I**) in mice with ALI (*n*=5). Bar = 20 μm. ApoV treatment decreased the levels of these cytokines. The lower panels show magnified images of the boxed areas in the upper panels (**B, H, I**). *P < 0.05, **P < 0.01, ***P < 0.001, ****P < 0.0001.

systemic infusion at 24 hours post-administration (Figure S2E). In addition, intratracheal administration of apoVs is more convenient and noninvasive, so we chose it as the optimal approach for apoV treatment in subsequent experiments.

Radiographic imaging, particularly computed tomography (CT) scanning, is essential for the diagnosis of ALI/ARDS.[34] Our CT scans revealed that mice with ALI exhibited lobar consolidations and ground-glass opacities in the lungs, whereas the images from normal mice were clear and lucent. ApoVs notably rescued the radiological appearance of the lungs in mice with ALI (Figure 1F). ALI/ARDS is associated with the accumulation of proinflammatory cytokines and decreased levels of anti-inflammatory cytokines,[35,36] and our findings showed that apoV treatment significantly increased the serum level of the anti-inflammatory cytokine IL-10 (Figure 1G). Additionally, immunofluorescence staining revealed strong accumulation of the proinflammatory cytokines TNF-α and IL-6 in the lung tissue of mice with ALI (Figure 1H and I); this accumulation was significantly reduced after apoV treatment (Figure 1H and I). These results demonstrate that apoV treatment can ameliorate lung injury in mice with ALI.

ApoVs Inhibited Neutrophil Infiltration and NETosis in the Lung Tissue of Mice with ALI

The immune response is a critical element in the progression of ALI/ARDS. Specifically, neutrophils play a central role in ALI.[15,16] Therefore, we evaluated the changes in neutrophils in the lung tissue of mice with ALI. The results revealed a dramatic increase in the proportion of Ly6G^{+}CD11b^{+} neutrophils, whereas treatment with apoV reversed this increase

in neutrophil abundance (Figure 2A). In addition, the protein expression of Ly6G was increased in the lung tissue of mice with ALI and was suppressed by apoV treatment, as determined by Western blotting (Figure 2B). Immunohistochemical staining and immunofluorescence staining further demonstrated that the accumulation of Ly6G$^+$ neutrophils in the lung tissue of mice with ALI was significantly reduced by apoV treatment (Figure 2C and D).

Morphological analysis of neutrophils by confocal microscopy revealed that most of the neutrophils in the lungs of mice with ALI displayed ruptured nuclear envelopes with release of decondensed chromatin, suggesting the occurrence of NETosis. ApoV treatment reversed this accumulation of NETotic neutrophils (Figure 2E). The results of Western blotting and immunostaining analysis supported this finding, as the expression of the NETosis markers MPO and H3Cit was increased in mice with ALI but subsequently decreased by apoV treatment (Figure 2F and G). Flow cytometry further verified that the number of Ly6G and H3Cit double-positive NETotic neutrophils in lung tissues was increased in mice with ALI but significantly reduced after apoV treatment (Figure 2H). Excessive NET formation can cause damage to the host.[19] These results indicated that apoV treatment may ameliorate lung injury in mice with ALI by repressing neutrophil infiltration and NETosis.
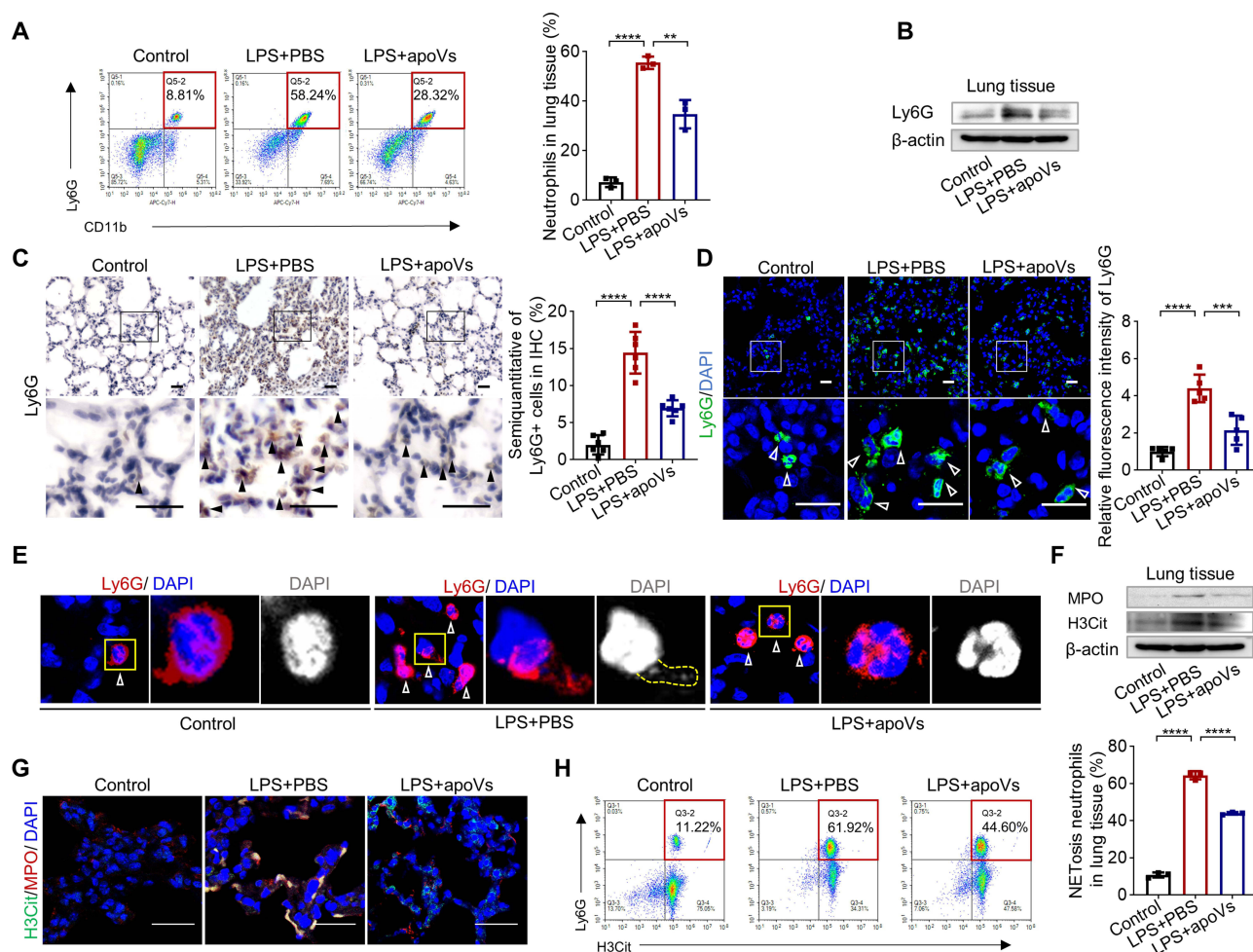

Figure 2 ApoVs decreased neutrophil infiltration and NETosis in the lungs of mice with ALI. (**A**) Neutrophils in lung tissue were quantified by flow cytometry. Ly6G and CD11b double-positive cells were gated as neutrophils (*n*=3). (**B**) Ly6G protein expression in lung tissue was analyzed by Western blotting. (**C**) Immunohistochemical staining of neutrophils in lung samples. Bar = 20 μm. Arrow heads indicate neutrophils (*n*=6). (**D**) Immunofluorescence staining of neutrophils in lung tissue samples (*n*=5). Bar = 20 μm. Arrow heads indicate neutrophils. The lower panels show magnified images of the boxed areas in the upper panels (**C, D**). (**E**) Morphological analysis of neutrophils by confocal microscopy revealed that most of the neutrophils in the lung tissue of mice with ALI occurred NETosis. Arrow heads indicate neutrophils. The boxed area in the left image is magnified in the right image. (**F**) Western blot analysis of NETosis-related proteins in lung tissue. (**G**) Immunofluorescence staining of neutrophil NETosis in lung samples. Bar = 20 μm. (**H**) Flow cytometry analysis of the neutrophil NETosis rate in lung tissue (*n*=3). **P < 0.01, ***P < 0.001, ****P < 0.0001.

ApoVs Suppressed Platelet Activation, Neutrophil-Platelet Aggregate (NPA) Formation and Platelet-Mediated NETosis

It has been previously established that platelet activation is a key factor in the adhesion of neutrophils to platelets, as they lead to the formation of NPAs and subsequently increase neutrophil influx into the lung during ALI/ARDS.[37,38] In addition, platelet activation promotes NETosis. To explore the potential of apoVs to suppress platelet activation and NPA formation, we conducted immunofluorescence analysis of lung tissue. Our results showed that mice with ALI exhibited an increased number of Ly6G and CD61 double-positive NPAs and CD61$^+$ platelets (Figure 3A). In contrast, apoV treatment markedly decreased the number of NPAs and platelets. Additionally, apoV treatment reversed the decrease in
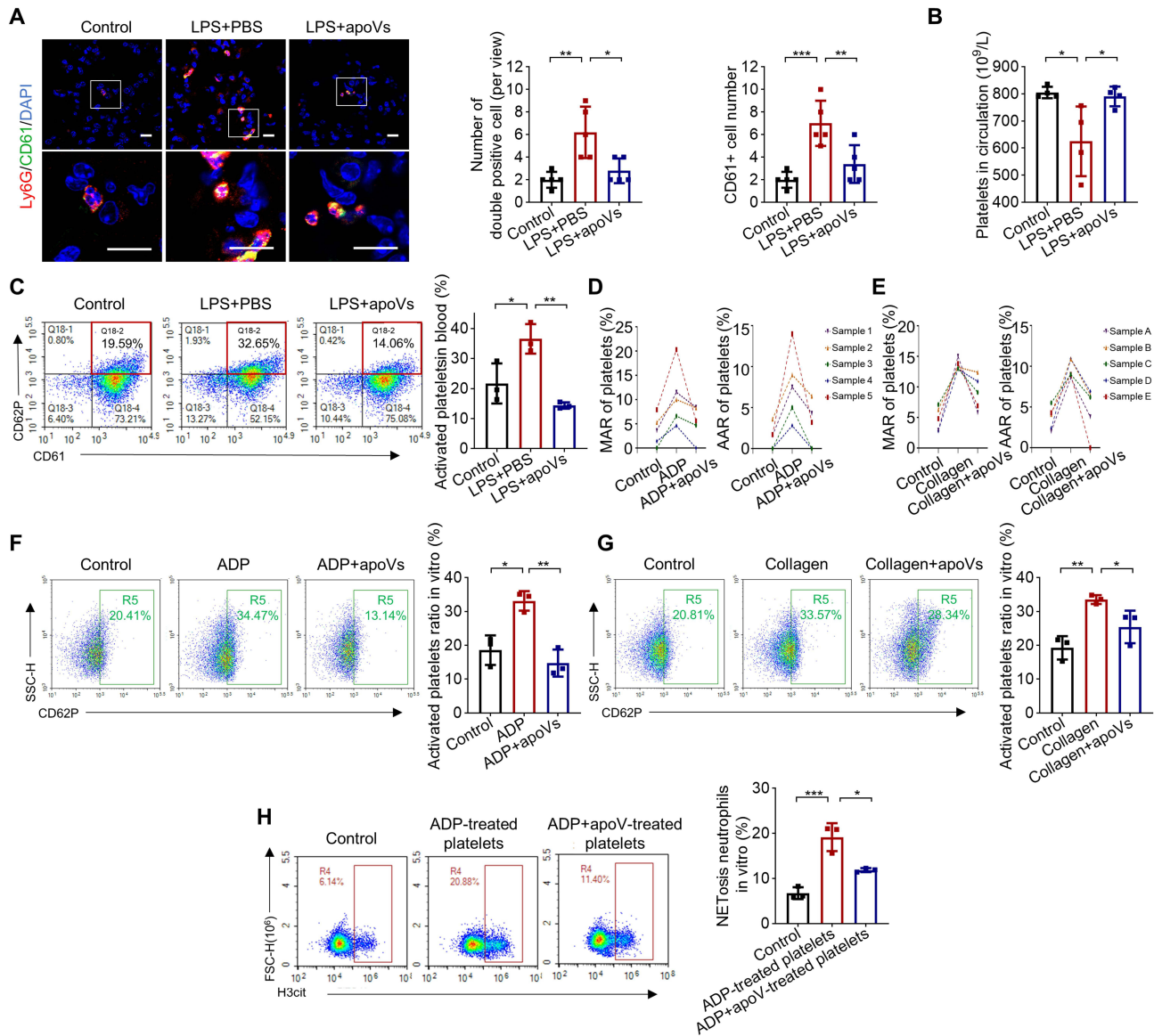

Figure 3 ApoVs inhibited platelet activation, NPA formation and platelet-mediated NETosis. (**A**) Immunofluorescence analysis of NPAs in lung tissues showed that apoV treatment decreased the number of NPAs and platelets in the lung tissue compared with that in the mice with ALI (*n*=5). Ly6G and CD61 double-positive cells were gated as NPAs. CD61-positive cells were gated as platelets. The lower panels show magnified images of the boxed areas in the upper panels. Bar = 20 μm. (**B**) Alterations in blood platelet counts were detected with an automated blood cell counter. ApoV treatment reversed the decrease in the number of circulating platelets in mice with ALI (*n*=4). (**C**) Platelet activation in vivo was detected by flow cytometry. Activated platelets were indicated by double positivity for CD61 and CD62P (*n*=3). (**D**) The Maximum aggregation rate (MAR) and average aggregation rate (AAR) of platelets activated by ADP in vitro (*n*=5). (**E**) The MAR and AAR of platelets activated by collagen in vitro (*n*=5). (**F**) Flow cytometry analysis of platelet activation stimulated by ADP and apoV treatment in vitro (*n*=3). (**G**) Flow cytometry analysis of platelet activation stimulated by collagen and apoV treatment in vitro (*n*=3). (**H**) Neutrophils were treated with different platelets, then NETosis ratio were analyzed with flow cytometry analysis. ApoV treatment repressed NETosis induced by activated platelets (*n*=3). *P < 0.05, **P < 0.01, ***P < 0.001.

the number of circulating platelets observed in mice with ALI (Figure 3B). This suggests that the formation of NPAs in ALI may consume circulating platelets, and apoV treatment can suppress the formation of NPAs in lung tissues, thereby decreasing the consumption of circulating platelets during ALI.

CD62P has been reported to facilitate platelet activation and the subsequent adhesion of neutrophils to platelets.[39,40] To assess the effect of apoVs on platelet activation in vivo, we employed flow cytometry analysis with CD62P and CD61 staining. Our findings revealed that apoV treatment significantly reduced the proportion of activated platelets in the blood of mice with ALI (Figure 3C). As platelet activation is strongly linked to platelet aggregation,[41] we further evaluated the effect of apoVs on platelet aggregation in vitro. ADP or collagen was used to induce platelet aggregation (Figure 3D and E). As expected, apoV treatment decreased the platelet aggregation induced by ADP or collagen (Figure 3D and E). Flow cytometry analysis confirmed that the ADP- or collagen-induced increases in activated platelet ratios were markedly inhibited by apoV treatment (Figure 3F and G). To examine the effect of activated platelets on NETosis, we established an in vitro coculture system with platelets and neutrophils. The results showed that platelets activated by ADP could trigger NETosis; however, when pretreated with apoVs and ADP, platelets displayed a reduced capacity to induce NETosis, as determined by H3Cit staining of neutrophils via flow cytometry analysis (Figure 3H). Taken together, these results suggest that apoVs may inhibit platelet activation during ALI, thereby suppressing neutrophil infiltration and NETosis.

ApoV-Mediated Inhibition of Platelet Activation and Neutrophil NETosis is Dependent on CD73

It has been reported previously that MSCs primarily inhibit platelet activation by regulating adenosine metabolism.[24] Adenosine metabolites are crucial signaling molecules for platelet function. Adenosine triphosphate (ATP) and ADP promote platelet activation, whereas adenosine inhibits platelet activation.[42] Therefore, we analyzed all the proteins of hBMMSC apoVs (proteomic analysis data were obtained from published research[43]) and genes involved in adenosine metabolism. The results revealed that 3 proteins in apoVs are involved in adenosine metabolic processes (Figure 4A), among which CD73 exhibited the highest expression (Figure 4B). CD73 is an enzyme that catalyzes the conversion of extracellular adenosine monophosphate (AMP) to adenosine. Previous research has shown that MSCs can inhibit platelet activation through CD73-converted adenosine.[24] Therefore, we detected CD73 expression on apoVs and found that apoVs had higher CD73 protein expression than MSCs (Figure 4C). According to these results, we hypothesized that apoVs might repress platelet activation and neutrophil NETosis through CD73. To test this hypothesis, $CD73^{KD}$-MSCs were generated and used to obtain $CD73$-knockdown apoVs ($CD73^{KD}$-apoVs) (Figure 4D-G). We confirmed the effect of CD73 on apoV-mediated inhibition of platelet activation by using $CD73^{KD}$-apoVs and a CD73 inhibitor and found that $CD73^{KD}$-apoVs and apoVs pretreated with a CD73 inhibitor showed a diminished capacity to inhibit platelet activation and aggregation (Figure 4H and I). Additionally, both $CD73^{KD}$-apoVs and apoVs pretreated with a CD73 inhibitor showed a comparatively reduced ability to inhibit activated platelet-induced NETosis in vitro, as indicated by flow cytometry (Figure 4J). These results suggest that apoV-mediated suppression of platelet activation and NETosis is dependent on CD73.

ApoVs Inhibited NETosis and Neutrophil Infiltration and Subsequently Attenuated Lung Injury in Mice with ALI Through CD73

To better understand the role of CD73 in apoV-mediated inhibition of NETosis in vivo, we treated mice with ALI with apoVs and $CD73^{KD}$-apoVs. Our results revealed that compared with apoVs, $CD73^{KD}$-apoVs failed to reduce neutrophil NETosis, as indicated by double-positive staining for Ly6G and H3Cit via flow cytometry (Figure 5A). Moreover, we discovered that $CD73^{KD}$-apoVs were unable to inhibit the accumulation of $Ly6G^+$ neutrophils in the lung tissue of mice with ALI, as determined by immunofluorescence staining and flow cytometry (Figure 5B and C).

Furthermore, we investigated whether CD73 is required for the apoV-mediated therapeutic effect on ALI. Our results showed that $CD73^{KD}$-apoVs failed to rescue lung injury, as assessed by H&E staining and lung injury scores (Figure 6A and B). $CD73^{KD}$-apoVs displayed an impaired capacity to rescue lung alveolar-capillary membrane injury in mice with
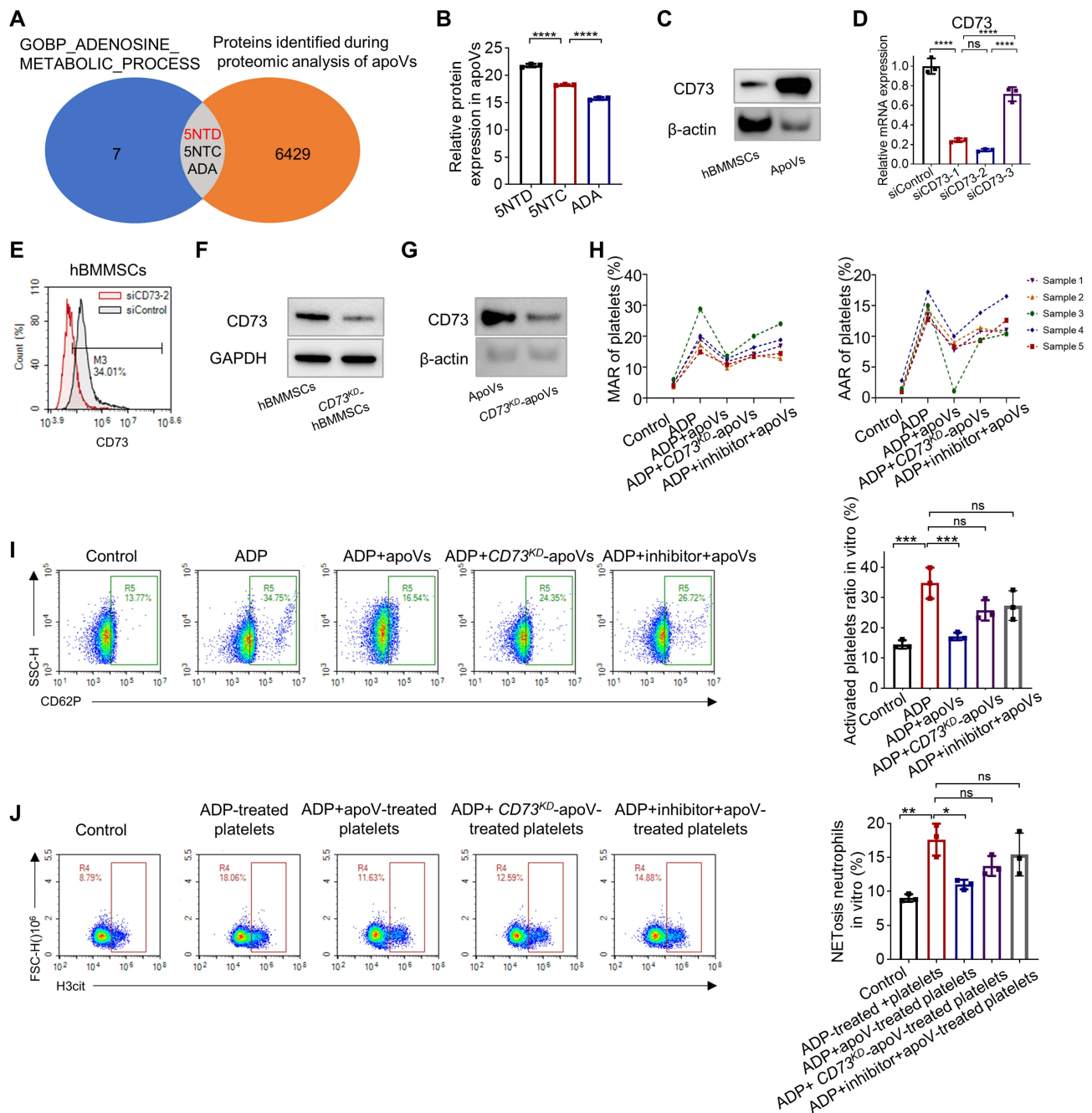
Figure 4 ApoV-mediated inhibition of platelet activation and neutrophil NETosis is dependent on CD73. (**A**) Venn diagrams showing the proteins shared between apoVs and adenosine metabolic processes. (**B**) The relative protein expression levels of 3 adenosine metabolic enzymes in apoVs (*n*=3). (**C**) The expression of CD73 on BMMSCs and apoVs. (**D**)-(**F**) The mRNA expression (*n*=3) (**D**) and protein expression (**E, F**) of CD73 on BMMSCs and *CD73^KD*-BMMSCs. (**G**) The protein expression of CD73 on apoVs and *CD73^KD*-apoVs. (**H**) The maximum aggregation rate (MAR) and average aggregation rate (AAR) of platelets activated in vitro (*n*=5). (**I**) Platelet activation was stimulated by ADP and inhibited by apoVs, while *CD73^KD*-apoV and apoVs pretreated with a CD73 inhibitor showed a diminished capacity to inhibit platelet activation (*n*=3). (**J**) Flow cytometry analysis of NETosis in vitro (*n*=3). *P < 0.05, **P < 0.01, ***P < 0.001, ****P < 0.0001, ns, not significant.

ALI, as assessed by the lung wet/dry ratio and total protein concentration in the BALF (Figure 6C and D). Subsequently, we used immunofluorescence staining to confirm the role of CD73 in apoV-mediated anti-inflammatory effects in the lungs of mice with ALI (Figure 6E and F). The results revealed that compared with apoVs, *CD73^KD*-apoVs had a reduced capacity to inhibit the production of TNF-α and IL-6 in the lung tissue of mice with ALI. Collectively, our results suggest that the therapeutic effect of apoVs on ALI is largely dependent on CD73.
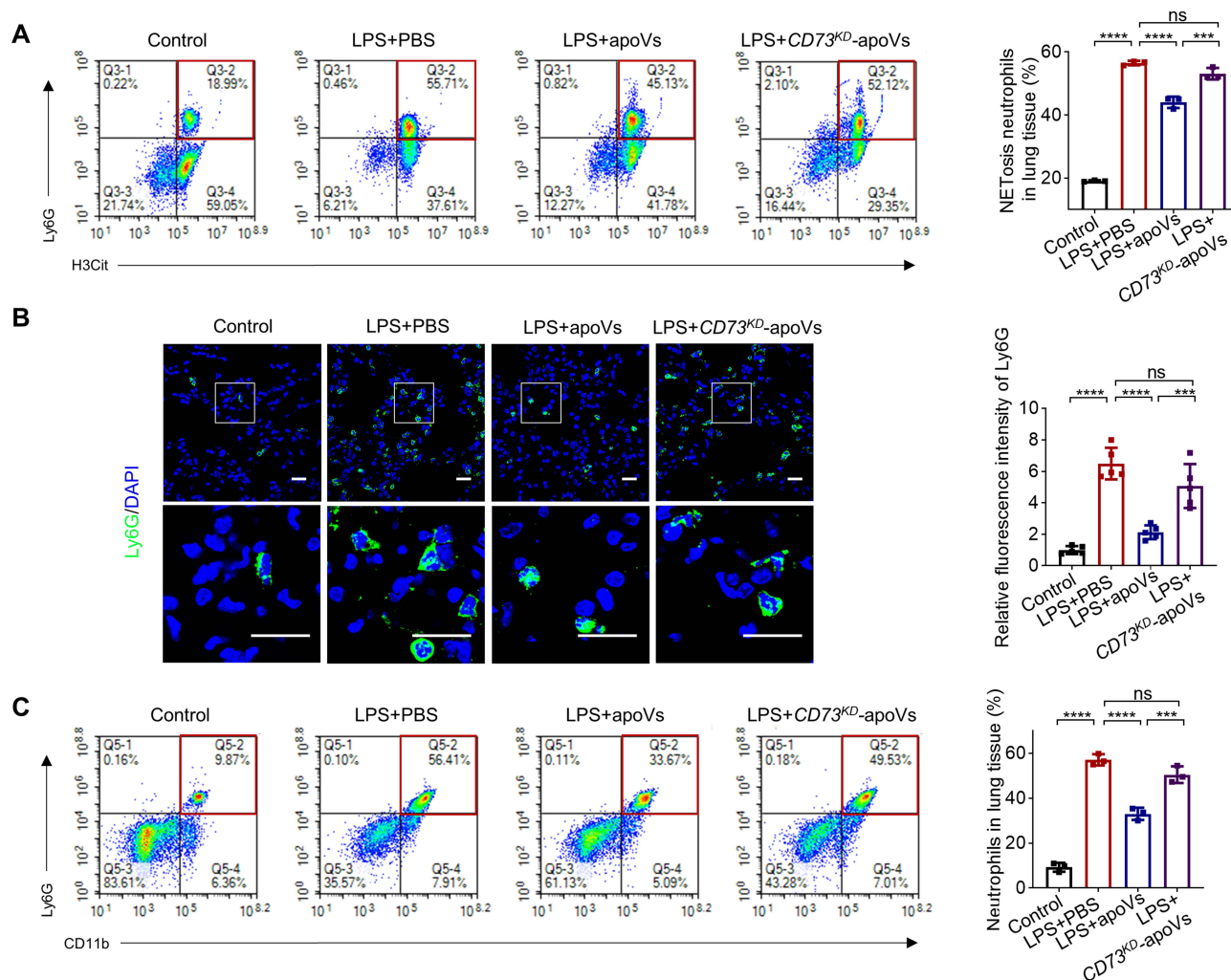
Figure 5 ApoVs inhibited NETosis and neutrophil infiltration in the lungs of mice with ALI through CD73. (**A**) NETosis neutrophil ratio in the lung tissue (*n*=3). (**B**) Immunofluorescence staining of neutrophils in lung tissue samples (*n*=5). Bar = 20 μm. The lower panels show magnified images of the boxed areas in the upper panels. (**C**) Flow cytometry analysis of neutrophil numbers in the lung tissue (*n*=3). ***P < 0.001, ****P < 0.0001; ns, not significant.

Discussion

MSCs have been shown to attenuate ALI through anti-inflammatory, immunomodulatory, and tissue repair effects.[44–48] However, MSC therapy still faces various challenges, such as safety, scalability, consistency, regulatory issues, and limited cell resources.[49] As an alternative treatment, cell-free therapeutics such as exosomes derived from MSCs have been proposed to reduce inflammation, promote the restoration of leaky epithelial membranes, and reduce sequelae of the cytokine storm.[50–52] Nevertheless, the low yield of exosomes results in a high cost of production, which also limits their application. Most studies report that an effective dose of exosomes ranges from 10–100 μg of exosomal protein per mouse, but less than 1 μg of protein can typically be extracted from 1 mL of culture medium, making large-scale production expensive.[53] In contrast, apoVs offer a simpler and more cost-effective alternative, with higher yields that facilitate large-scale production and application. ApoVs have been demonstrated to have therapeutic effects in a variety of contexts, including osteopenia, multiple myeloma, wound healing and sepsis.[13,14,54,55] Our study found that MSC-derived apoVs may be a viable therapy for ALI/ARDS. Furthermore, intratracheal administration allows apoVs to enter the inflammatory site directly, thus improving administration efficiency and providing a more convenient and noninvasive option for clinical application.

Neutrophils are essential for inflammation in ALI/ARDS,[56] and severe cases of ALI/ARDS are always accompanied by increased neutrophil infiltration and NETosis.[2,16,57] Transmigrated neutrophils release granule proteins, such as
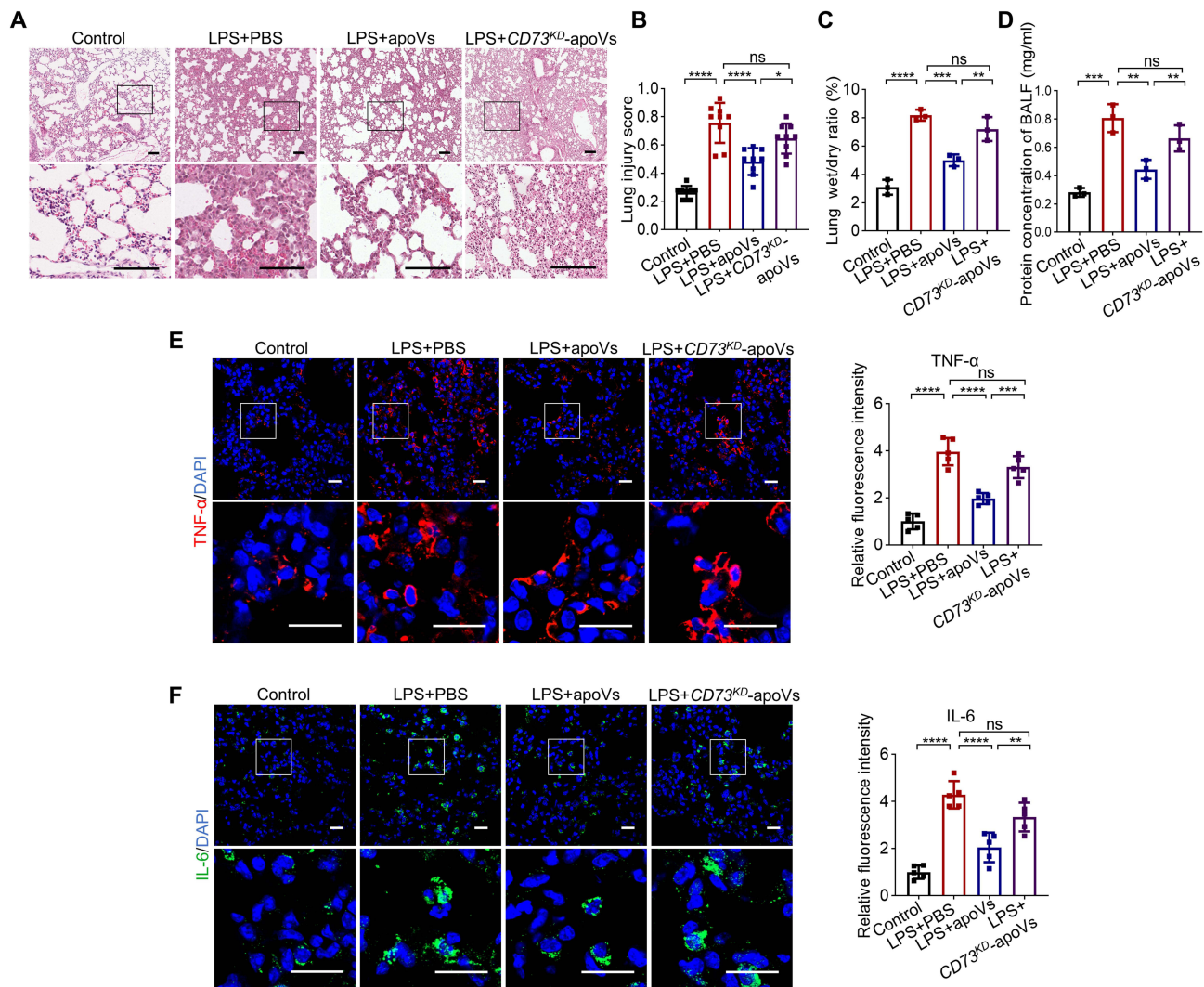
Figure 6 ApoVs attenuated lung injury in mice with ALI through CD73. (**A**) Representative H&E staining images of lung samples from the different groups. Bar = 100 μm. (**B**) The lung injury score showed that *CD73* [KD]-apoVs failed to reverse lung injury (*n*=9). (**C**) The lung wet/dry weight ratio (*n*=3). (**D**) Protein concentrations in BALF from different groups (*n*=3). (**E, F**) Immunofluorescence staining of lung samples revealed that *CD73* [KD]-apoVs failed to suppress the high concentrations of TNF-α (**E**) and IL-6 (**F**) observed in mice with ALI (*n*=5). Bar = 20 μm. The lower panels show magnified images of the boxed areas in the upper panels (**A, E, F**). *P < 0.05, **P < 0.01, ***P < 0.001, ****P < 0.0001, ns, not significant.

elastases, matrix metalloproteinases, and cationic polypeptides, which further exacerbate ALI/ARDS.[58] NETosis can also aggravate ALI/ARDS.[20] Therefore, neutrophil depletion or inhibition of neutrophil NETosis may be beneficial for reducing inflammation in ALI/ARDS.[59,60] Our previous study revealed that apoVs can switch from neutrophil NETosis to apoptosis, thereby attenuating sepsis.[55] In this study, we further revealed that apoVs not only suppress NETosis in neutrophils but also impede the chemotaxis of neutrophils into the lungs, thus alleviating inflammatory injury in mice with ALI. Our results demonstrate the multiple regulatory effects of apoV on neutrophils, providing a potential therapeutic approach for ALI/ARDS.

During ALI/ARDS, platelets are activated and interact with neutrophils to form NPAs,[23] which can facilitate neutrophil-endothelial interactions at sites of inflammation, resulting in the recruitment of neutrophils to the lung.[61] Furthermore, activated platelets have also been shown to stimulate NETosis in ALI.[62] The activation of platelets is initiated by interactions with collagen or platelet agonists (such as ADP) that engage G protein-coupled receptors. This leads to the release of large amounts of ADP, which in turn enhances coagulation and can be converted to AMP by platelet CD39 activity.[63] Our study showed that apoVs inhibit platelet activation and that the subsequent infiltration and NETosis of neutrophils depend on CD73. CD73 catalyzes the conversion of AMP to adenosine, which activates A2A

receptors (A2AR) and other P1 receptors, increasing cAMP levels and phosphorylating vasodilator-stimulated phospho-protein (VASP). This signaling pathway halts the activation cascade and reduces excessive platelet reactivity.[24] This may be the underlying mechanism by which apoVs inhibit platelet activation. Our findings indicate that the therapeutic effects of apoVs on ALI/ARDS also depend on CD73. It is noteworthy that CD73 plays a critical role not only in regulating platelet activity but also in modulating various immune cells. Studies have shown that CD73 inhibits neutrophil activation, promotes macrophage polarization towards the M2 phenotype, suppresses T cell activity, enhances regulatory T cell (Treg) differentiation, induces the expression of immunosuppressive receptors on dendritic cells, and reduces the cytotoxicity of natural killer cells.[64–66] This study primarily examines the regulatory effects of apoVs on platelets and neutrophils via CD73. However, further research is warranted to determine whether apoVs also influence other immune cells within the ALI inflammatory microenvironment.

Conclusion

Our findings suggest that apoVs can attenuate lung injury in ALI by suppressing platelet activation and, as a result, suppressing neutrophil infiltration and NETosis. The modulation of platelet activation is mediated by CD73. This study highlighted the therapeutic potential of apoVs for ALI/ARDS and revealed the multiple regulatory effects of apoVs on neutrophils, providing a new perspective for the treatment of ALI/ARDS.

Data Sharing Statement

The datasets supporting the conclusions of this article are included within the article and its additional file, and further inquiries can be directed to the corresponding author.

Acknowledgments

Disclosure

The authors declare no potential conflicts of interest in this work.

References

1. Jiang F, Deng L, Zhang L, Cai Y, Cheung CW, Xia Z. Review of the clinical characteristics of coronavirus disease 2019 (covid-19). *J Gen Intern Med*. 2020;35(5):1545–1549. doi:10.1007/s11606-020-05762-w
2. Thompson BT, Chambers RC, Liu KD. Acute respiratory distress syndrome. *N Engl J Med*. 2017;377(6):562–572. doi:10.1056/NEJMra1608077
3. Meyer NJ, Gattinoni L, Calfee CS. Acute respiratory distress syndrome. *Lancet*. 2021;398(10300):622–637. doi:10.1016/S0140-6736(21)00439-6
4. Herridge MS, Tansey CM, Matte A, et al. Functional disability 5 years after acute respiratory distress syndrome. *N Engl J Med*. 2011;364 (14):1293–1304. doi:10.1056/NEJMoa1011802
5. Horie S, Masterson C, Devaney J, Laffey JG. Stem cell therapy for acute respiratory distress syndrome: a promising future? *Curr Opin Crit Care*. 2016;22(1):14–20. doi:10.1097/MCC.0000000000000276
6. Walter J, Ware LB, Matthay MA. Mesenchymal stem cells: mechanisms of potential therapeutic benefit in ards and sepsis. *Lancet Respir Med*. 2014;2(12):1016–1026. doi:10.1016/S2213-2600(14)70217-6
7. Lee JW, Fang X, Krasnodembskaya A, Howard JP, Matthay MA. Concise review: mesenchymal stem cells for acute lung injury: role of paracrine soluble factors. *Stem Cells*. 2011;29(6):913–919. doi:10.1002/stem.643
8. Nemeth K, Leelahavanichkul A, Yuen PS, et al. Bone marrow stromal cells attenuate sepsis via prostaglandin e(2)-dependent reprogramming of host macrophages to increase their interleukin-10 production. *Nat Med*. 2009;15(1):42–49. doi:10.1038/nm.1905
9. Martinez-Gonzalez I, Roca O, Masclans JR, et al. Human mesenchymal stem cells overexpressing the il-33 antagonist soluble il-1 receptor-like-1 attenuate endotoxin-induced acute lung injury. *Am J Respir Cell Mol Biol*. 2013;49(4):552–562. doi:10.1165/rcmb.2012-0406OC
10. Liu S, Jiang L, Li H, et al. Mesenchymal stem cells prevent hypertrophic scar formation via inflammatory regulation when undergoing apoptosis. *J Invest Dermatol*. 2014;134(10):2648–2657. doi:10.1038/jid.2014.169
11. Galleu A, Riffo-Vasquez Y, Trento C, et al. Apoptosis in mesenchymal stromal cells induces in vivo recipient-mediated immunomodulation. *Sci Transl Med*. 2017;9(416). doi:10.1126/scitranslmed.aam7828
12. Gyorgy B, Szabo TG, Pasztoi M, et al. Membrane vesicles, current state-of-The-art: emerging role of extracellular vesicles. *Cell Mol Life Sci*. 2011;68(16):2667–2688. doi:10.1007/s00018-011-0689-3
13. Liu D, Kou X, Chen C, et al. Circulating apoptotic bodies maintain mesenchymal stem cell homeostasis and ameliorate osteopenia via transferring multiple cellular factors. *Cell Res*. 2018;28(9):918–933. doi:10.1038/s41422-018-0070-2

 105

14. Wang J, Cao Z, Wang P, et al. Apoptotic extracellular vesicles ameliorate multiple myeloma by restoring fas-mediated apoptosis. *Acs Nano*. 2021;15(9):14360–14372. doi:10.1021/acsnano.1c03517

15. Matthay MA, Ware LB, Zimmerman GA. The acute respiratory distress syndrome. *J Clin Invest*. 2012;122(8):2731–2740. doi:10.1172/JCI60331

16. Lefrancais E, Mallavia B, Zhuo H, Calfee CS, Looney MR. Maladaptive role of neutrophil extracellular traps in pathogen-induced lung injury. *JCI Insight*. 2018;3(3). doi:10.1172/jci.insight.98178

17. Juss JK, House D, Amour A, et al. Acute respiratory distress syndrome neutrophils have a distinct phenotype and are resistant to phosphoinositide 3-kinase inhibition. *Am J Respir Crit Care Med*. 2016;194(8):961–973. doi:10.1164/rccm.201509-1818OC

18. Juss J, Herre J, Begg M, et al. Genome-wide transcription profiling in neutrophils in acute respiratory distress syndrome. *Lancet*. 2015;385(Suppl 1):S55. doi:10.1016/S0140-6736(15)60370-1

19. Gupta S, Sahni V. The intriguing commonality of netosis between covid-19 & periodontal disease. *Med Hypotheses*. 2020;144:109968. doi:10.1016/j.mehy.2020.109968

20. Diniz L, Matsuba BK, Souza P, et al. Effects of neutrophil extracellular traps during human respiratory syncytial virus infection in vitro. *Braz J Biol*. 2021;83:e248717. doi:10.1590/1519-6984.248717.

21. Andrews RK, Arthur JF, Gardiner E. Neutrophil extracellular traps (nets) and the role of platelets in infection. *Thromb Haemost*. 2014;112(4):659–665. doi:10.1160/TH-14-05-0455

22. Higashikuni Y, Liu W, Obana T, Sata M. Pathogenic basis of thromboinflammation and endothelial injury in covid-19: current findings and therapeutic implications. *Int J Mol Sci*. 2021;22(21):12081. doi:10.3390/ijms222112081

23. Chang YW, Tseng CP, Lee CH, et al. Beta-nitrostyrene derivatives attenuate lps-mediated acute lung injury via the inhibition of neutrophil-platelet interactions and net release. *Am J Physiol Lung Cell Mol Physiol*. 2018;314(4):L654–L669. doi:10.1152/ajplung.00501.2016

24. Netsch P, Elvers-Hornung S, Uhlig S, et al. Human mesenchymal stroma l cells inhibit platelet activation and aggregation involving cd73-converted adenosine. *Stem Cell Res Ther*. 2018;9(1):184. doi:10.1186/s13287-018-0936-8

25. Mendelson A, Strat AN, Bao W, et al. Mesenchymal stromal cells lower platelet activation and assist in platelet formation in vitro. *JCI Insight*. 2019;4(16). doi:10.1172/jci.insight.126982

26. Hashi CK, Zhu Y, Yang GY, et al. Antithrombogenic property of bone marrow mesenchymal stem cells in nanofibrous vascular grafts. *Proc Natl Acad Sci U S A*. 2007;104(29):11915–11920. doi:10.1073/pnas.0704581104

27. Zhong EH, Ledderose C, De Andrade MP, et al. Structural and functional characterization of engineered bifunctional fusion proteins of cd39 and cd73 ectonucleotidases. *Am J Physiol Cell Physiol*. 2021;320(1):C15–C29. doi:10.1152/ajpcell.00430.2020

28. Kaspi H, Semo J, Abramov N, et al. Msc-ntf (nurown(r)) exosomes: a novel therapeutic modality in the mouse lps-induced ards model. *Stem Cell Res Ther*. 2021;12(1):72. doi:10.1186/s13287-021-02143-w

29. Pedrazza L, Cunha AA, Luft C, et al. Mesenchymal stem cells improves survival in lps-induced acute lung injury acting through inhibition of nets formation. *J Cell Physiol*. 2017;232(12):3552–3564. doi:10.1002/jcp.25816

30. Xing D, Wells JM, Giordano SS, et al. Induced pluripotent stem cell-derived endothelial cells attenuate lipopolysaccharide-induced acute lung injury. *J Appl Physiol (1985)*. 2019;127(2):444–456. doi:10.1152/japplphysiol.00587.2018

31. Sheahan TP, Sims AC, Leist SR, et al. Comparative therapeutic efficacy of remdesivir and combination lopinavir, ritonavir, and interferon beta against mers-cov. *Nat Commun*. 2020;11(1):222. doi:10.1038/s41467-019-13940-6

32. Zhang L, Hu X, Zhu J, et al. Adequate platelet function inhibition confirmed by two inductive agents predicts lower recurrence of ischemic stroke/transient ischemic attack. *Biomed Res Int*. 2017;2017:1–5. doi:10.1155/2017/3504950

33. Gao X, Lu S, Ge Z, et al. Relationship between high platelet reactivity on clopidogrel and long-term clinical outcomes after drug-eluting stents implantation (paint-des): a prospective, propensity score-matched cohort study. *Bmc Cardiovasc Disor*. 2018;18(1). doi:10.1186/s12872-018-0841-1

34. Sheard S, Rao P, Devaraj A. Imaging of acute respiratory distress syndrome. *Respir Care*. 2012;57(4):607–612. doi:10.4187/respcare.01731

35. Machado C, Gonzalez-Quevedo A. Hypoxemia and cytokine storm in covid-19: clinical implications. *Medicc Rev*. 2021;23(3–4):54–59. doi:10.37757/MR2021.V23.N3.10

36. Alghetaa H, Mohammed A, Zhou J, Singh N, Nagarkatti M, Nagarkatti P. Resveratrol-mediated attenuation of superantigen-driven acute respiratory distress syndrome is mediated by microbiota in the lungs and gut. *Pharmacol Res*. 2021;167:105548. doi:10.1016/j.phrs.2021.105548

37. Kuebler WM. Selectins revisited: the emerging role of platelets in inflammatory lung disease. *J Clin Invest*. 2006;116(12):3106–3108. doi:10.1172/JCI30664

38. Morris G, Bortolasci CC, Puri BK, et al. Preventing the development of severe covid-19 by modifying immunothrombosis. *Life Sci*. 2021;264:118617. doi:10.1016/j.lfs.2020.118617

39. Wallis S, Wolska N, Englert H, et al. A peptide from the staphylococcal protein efb binds p-selectin and inhibits the interaction of platelets with leukocytes. *J Thromb Haemost*. 2021;20(3):729–741. doi:10.1111/jth.15613

40. Zarbock A, Singbartl K, Ley K. Complete reversal of acid-induced acute lung injury by blocking platelet-neutrophil aggregation. *J Clin Invest*. 2006;116(12):3211–3219. doi:10.1172/JCI29499

41. Kim SJ, Carestia A, Mcdonald B, et al. Platelet-mediated net release amplifies coagulopathy and drives lung pathology during severe influenza infection. *Front Immunol*. 2021;12:772859. doi:10.3389/fimmu.2021.772859

42. Carminita E, Crescence L, Brouilly N, Altie A, Panicot-Dubois L, Dubois C. DNAse-dependent, net-independent pathway of thrombus formation in vivo. *Proc Natl Acad Sci U S A*. 2021;118(28). doi:10.1073/pnas.2100561118

43. Zhang X, Tang J, Kou X, et al. Proteomic analysis of msc-derived apoptotic vesicles identifies fas inheritance to ameliorate haemophilia a via activating platelet functions. *J Extracell Vesicles*. 2022;11(7):e12240. doi:10.1002/jev2.12240

44. Devaney J, Horie S, Masterson C, et al. Human mesenchymal stromal cells decrease the severity of acute lung injury induced by e Coli in the rat. *Thorax*. 2015;70(7):625–635. doi:10.1136/thoraxjnl-2015-206813

45. Hayes M, Masterson C, Devaney J, et al. Therapeutic efficacy of human mesenchymal stromal cells in the repair of established ventilator-induced lung injury in the rat. *Anesthesiology*. 2015;122(2):363–373. doi:10.1097/ALN.0000000000000545

46. Krasnodembskaya A, Song Y, Fang X, et al. Antibacterial effect of human mesenchymal stem cells is mediated in part from secretion of the antimicrobial peptide ll-37. *Stem Cells*. 2010;28(12):2229–2238. doi:10.1002/stem.544

47. Lee JW, Krasnodembskaya A, Mckenna DH, Song Y, Abbott J, Matthay MA. Therapeutic effects of human mesenchymal stem cells in ex vivo human lungs injured with live bacteria. *Am J Respir Crit Care Med*. 2013;187(7):751–760. doi:10.1164/rccm.201206-0990OC

48. Islam MN, Das SR, Emin MT, et al. Mitochondrial transfer from bone-marrow-derived stromal cells to pulmonary alveoli protects against acute lung injury. *Nat Med*. 2012;18(5):759–765. doi:10.1038/nm.2736

49. Metcalfe SM. Mesenchymal stem cells and management of covid-19 pneumonia. *Med Drug Discov.* 2020;5:100019. doi:10.1016/j.medidd.2020.100019

50. Lee JH, Park J, Lee JW. Therapeutic use of mesenchymal stem cell-derived extracellular vesicles in acute lung injury. *Transfusion*. 2019;59 (S1):876–883. doi:10.1111/trf.14838

51. Tang XD, Shi L, Monsel A, et al. Mesenchymal stem cell microvesicles attenuate acute lung injury in mice partly mediated by ang-1 mRNA. *Stem Cells*. 2017;35(7):1849–1859. doi:10.1002/stem.2619

52. Preda MB, Neculachi CA, Fenyo IM, et al. Short lifespan of syngeneic transplanted msc is a consequence of in vivo apoptosis and immune cell recruitment in mice. *Cell Death Dis*. 2021;12(6):566. doi:10.1038/s41419-021-03839-w

53. Xu B, Chen SS, Liu MZ, Gan CX, Li JQ, Guo GH. Stem cell derived exosomes-based therapy for acute lung injury and acute respiratory distress syndrome: a novel therapeutic strategy. *Life Sci*. 2020;254:117766. doi:10.1016/j.lfs.2020.117766

54. Liu J, Qiu X, Lv Y, et al. Apoptotic bodies derived from mesenchymal stem cells promote cutaneous wound healing via regulating the functions of macrophages. *Stem Cell Res Ther*. 2020;11(1):507. doi:10.1186/s13287-020-02014-w

55. Ou Q, Tan L, Shao Y, et al. Electrostatic charge-mediated apoptotic vesicle biodistribution attenuates sepsis by switching neutrophil netosis to apoptosis. *Small*. 2022;18(20):2200306. doi:10.1002/smll.202200306

56. Williams AE, Chambers RC. The mercurial nature of neutrophils: still an enigma in ards? *Am J Physiol Lung Cell Mol Physiol*. 2014;306(3):L217–L230. doi:10.1152/ajplung.00311.2013

57. Li H, Zhou X, Tan H, et al. Neutrophil extracellular traps contribute to the pathogenesis of acid-aspiration-induced ali/ards. *Oncotarget*. 2018;9 (2):1772–1784. doi:10.18632/oncotarget.22744

58. Frantzeskaki F, Armaganidis A, Orfanos SE. Immunothrombosis in acute respiratory distress syndrome: cross talks between inflammation and coagulation. *Respiration*. 2017;93(3):212–225. doi:10.1159/000453002

59. Sercundes MK, Ortolan LS, Debone D, et al. Targeting neutrophils to prevent malaria-associated acute lung injury/acute respiratory distress syndrome in mice. *PLoS Pathog*. 2016;12(12):e1006054. doi:10.1371/journal.ppat.1006054

60. Lucas CD, Dorward DA, Tait MA, et al. Downregulation of mcl-1 has anti-inflammatory pro-resolution effects and enhances bacterial clearance from the lung. *Mucosal Immunol*. 2014;7(4):857–868. doi:10.1038/mi.2013.102

61. Chen WA, Fletcher HM, Payne KJ, et al. Platelet and neutrophil responses to porphyromonas gingivalis in human whole blood. *Mol Oral Microbiol*. 2021;36(3):202–213. doi:10.1111/omi.12336

62. Burkard P, Schonhart C, Vogtle T, et al. A key role for platelet gpvi in neutrophil recruitment, migration and netosis in the early stages of acute lung injury. *Blood*. 2023;142(17):1463–1477. doi:10.1182/blood.2023019940

63. Estevez B, Du X. New concepts and mechanisms of platelet activation signaling. *Physiology (Bethesda)*. 2017;32(2):162–177. doi:10.1152/physiol.00020.2016

64. Nakao Y, Fukuda T, Zhang Q, et al. Exosomes from tnf-α-treated human gingiva-derived MSCs enhance M2 macrophage polarization and inhibit periodontal bone loss. *Acta Biomater*. 2021;122:306–324. doi:10.1016/j.actbio.2020.12.046

65. Zhou Y, Kang L, Yin G, et al. Adenosine a2b receptor activation regulates the balance between t helper 17 cells and regulatory t cells, and inhibits regulatory t cells exhaustion in experimental autoimmune myositis. *J Cachexia, Sarcopenia Muscle*. 2024;15(6):2460–2475. doi:10.1002/jcsm.13581

66. Gardani C, Diz FM, Donde LB, Rockenbach L, Laufer S, Morrone FB. The potential role of purinergic signaling in cancer therapy: perspectives on anti-cd73 strategies for prostate cancer. *Front Immunol*. 2024;15:1455469. doi:10.3389/fimmu.2024.1455469

107